How to cite: *Angew. Chem. Int. Ed.* **2024**, *63*, e202402025
doi.org/10.1002/anie.202402025

Nanoclusters

Diphosphine-Protected $IrAu_{12}$ Superatom with Open Site(s): Synthesis and Programmed Stepwise Assembly

*Yuto Fukumoto[+], Tsubasa Omoda[+], Haru Hirai, Shinjiro Takano, Koji Harano, and Tatsuya Tsukuda**

Abstract: One or two phenylacetylide (PA) ligand(s) were successfully removed from the $IrAu_{12}$ superatomic core of $[IrAu_{12}(dppe)_5(PA)_2]^+$ (dppe = 1,2-bis(diphenylphosphino)ethane) by reaction with controlled amounts of tetrafluoroboric acid. Optical and nuclear magnetic resonance spectroscopies and density functional theory calculations revealed the formation of open Au site(s) on the $IrAu_{12}$ core of $[IrAu_{12}(dppe)_5(PA)_1]^{2+}$ and $[IrAu_{12}(dppe)_5]^{3+}$ with the remaining structure intact. Isocyanide was efficiently trapped at the open electrophilic site on $[IrAu_{12}(dppe)_5(PA)_1]^{2+}$, whereas a dimer or trimer of the $IrAu_{12}$ superatoms was formed using diisocyanide as a linker. These results open the door to designed assembly of chemically modified metal superatoms.

Introduction

Chemically modified gold superatoms (Au CMSs) are a new class of nanosized molecules that exhibit novel and diverse properties owing to the size-specific structures of the Au cores.[1–4] Au CMSs with crystallographically determined structures are promising candidates as (1) platforms for the study of structure–property correlations[4] and (2) building units of assembled materials.[5–9] In order to assemble Au CMSs via covalent bonding, ligand exchange reactions with multidentate ligands have been frequently used.[10–13] However, design and fabrication of controlled assembled structures are challenging because the number and position of exchangeable sites of Au CMSs are difficult to control. A promising approach to overcome this problem is to pre-install exposed sites on the Au CMSs whereby the Au CMSs are assembled into a programmed structure by multidentate ligands. Furthermore, such Au CMSs with partially exposed Au sites will offer new opportunities to investigate and tune their catalytic properties since the accessible sites of the substrate can be regulated at the molecular level.[14–16] One of the current strategies for creating exposed sites is reduction of the surface coverage by steric repulsion between bulky ligands.[17–20] For example, an Au_{23} cluster with naked sites catalyzed the oxidation reaction of benzyl alcohol.[19] However, as it is difficult to design and predict the number and position of exposed sites by such approaches, a new method is required for fabricating the exposed sites in a controlled manner.

The present study aimed to achieve this goal by the selective removal of anionic ligand(s) from the predefined CMSs. The platforms we chose for this purpose were $[Au_{13}(dppe)_5(PA)_2]^{3+}$, $[PdAu_{12}(dppe)_5(PA)_2]^{2+}$, and $[IrAu_{12}(dppe)_5(PA)_2]^+$, where dppe and PA–H represent 1,2-bis(diphenylphosphino)ethane and phenylacetylene, respectively. These clusters bear two anionic PA ligands at the opposite sites of an icosahedral $M@Au_{12}$ core (M = Au, Pd, Ir)[21–24] and will be referred to as $\mathbf{AuPA_2^{3+}}$, $\mathbf{PdPA_2^{2+}}$, and $\mathbf{IrPA_2^{+}}$, respectively, in terms of the dopant element, the number of PA ligand(s), and the total charge. Electrospray ionization mass spectrometry (ESI-MS) demonstrated that the PA ligands were removed stepwise only from $\mathbf{IrPA_2^{+}}$ to form $\mathbf{IrPA_1^{2+}}$ and $\mathbf{Ir^{3+}}$ by the reaction with strong Brønsted acid. The formation of an open site in $\mathbf{IrPA_1^{2+}}$ was confirmed by nuclear magnetic resonance (NMR) spectroscopy, density functional theory (DFT) calculations, and a trapping experiment with 1-isocyanoadamantane (IA). By taking advantage of the designed exposed sites on $\mathbf{IrPA_1^{2+}}$ and $\mathbf{Ir^{3+}}$, two or three $Ir@Au_{12}$ cores were linked linearly via 4,4″-*p*-terphenyldiisocyanide (L).

[*] Y. Fukumoto,[+] Prof. Dr. T. Omoda,[+] Dr. H. Hirai, Prof. Dr. S. Takano, Prof. Dr. T. Tsukuda
Department of Chemistry, Graduate School of Science
The University of Tokyo
7-3-1 Hongo, Bunkyo-ku, Tokyo 113-0033, Japan
E-mail: tsukuda@chem.s.u-tokyo.ac.jp

Prof. Dr. T. Omoda[+]
Present address: Department of Chemical Science and Engineering, School of Materials and Chemical Technology
Tokyo Institute of Technology
O-okayama, Meguro-ku, Tokyo 152-8552, Japan.

Prof. Dr. K. Harano
Center for Basic Research on Materials
National Institute for Materials Science,
1-1 Namiki, Tsukuba, Ibaraki 305-0044, Japan.

[+] These authors contributed equally to this work.

Results and Discussion

Synthesis and Structures of MPA_2 Clusters (M = Au, Pd, Ir)

Cluster $\mathbf{AuPA_2}^{3+}$ was synthesized by the reported methods.[21] Clusters $\mathbf{PdPA_2}^{2+}$ and $\mathbf{IrPA_2}^{+}$ were newly synthesized by the ligand exchange reaction[21] of $[PdAu_{12}(dppe)_5Cl_2]^{2+}$ and $[IrAu_{12}(dppe)_5Cl_2]^{+}$ (Refs. [22] and [24]) with PA–H, respectively.[25] Figure 1 and Table S1 show the single-crystal X-ray diffraction (SCXRD) results of $\mathbf{PdPA_2}^{2+}$ and $\mathbf{IrPA_2}^{+}$.[26,27] The structural motifs of $\mathbf{PdPA_2}^{2+}$ and $\mathbf{IrPA_2}^{+}$ were similar to that of $\mathbf{AuPA_2}^{3+}$ (Ref. [21]) and were composed of an icosahedral $M@Au_{12}$ (M = Pd or Ir) core capped by five dppe ligands and two PA ligands at the coaxial position. Two Au–C bonds in $\mathbf{PdPA_2}^{2+}$ (2.04 Å and 2.08 Å) and $\mathbf{IrPA_2}^{+}$ (2.03 Å and 2.16 Å) were not equivalent in the crystal (Figure 1), while a single peak in the $^{31}P\{^1H\}$ NMR chart in acetone-*d*6 (Figures S1a and S2) indicated that the two Au–C bonds were equivalent in solution. The average lengths of the Au–C bonds in $\mathbf{MPA_2}$ were 2.01, 2.06, and 2.10 Å for M = Au, Pd, and Ir, respectively. This trend suggests that the Au–C bond becomes weaker in the order of $\mathbf{AuPA_2}^{3+}$, $\mathbf{PdPA_2}^{2+}$, and $\mathbf{IrPA_2}^{+}$. Figure 2 summarizes other characterization results of $\mathbf{IrPA_2}^{+}$. The chemical composition and purity were confirmed by ESI-MS (Figure 2a, black). The UV/Vis absorption spectrum (Figure 2b, black) showed an onset at ~520 nm and clear peaks at ~310 and ~415 nm. The photoluminescence (PL) spectrum (Figure 2b, red) exhibited a band centered at ~615 nm with a PL quantum yield (QY) of 53 % in Ar. The ^1H NMR chart (black trace in Figure 2c, Figure S3) exhibited doublet peaks at ~7.8 ppm (peak a) due to ortho protons of the phenyl ring of PA ligands (a in Figure 2d) and a singlet peak at ~8.8 ppm (peak b) due to ortho protons of two equivalent phenyl rings of dppe ligands located at the axial position (b in Figure 2d). Figure 3a shows the DFT optimized structure of $[IrAu_{12}(dmpe)_5(PA)_2]^{+}$ ($\mathbf{IrPA_2\text{-}m}^{+}$), which was obtained by replacing dppe of $\mathbf{IrPA_2}^{+}$ with dmpe (1,2-bis(dimethylphosphino)ethane).[25] The optimized structure of $\mathbf{IrPA_2\text{-}m}^{+}$ reproduced the structural motif of $\mathbf{IrPA_2}^{+}$ (Figure 1c). According to the Kohn–Sham (KS) orbital analysis (Fig-

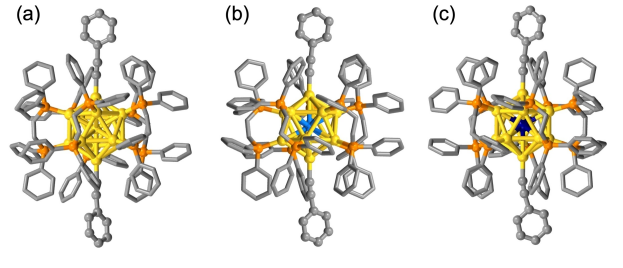

Figure 1. Crystal structures of (a) $\mathbf{AuPA_2}^{3+}$ (Ref. [21]) (b) $\mathbf{PdPA_2}^{2+}$, and (c) $\mathbf{IrPA_2}^{+}$. Solvent molecules, hydrogen atoms, and counter anions are omitted for clarity. Carbon atoms in dppe ligands are depicted as sticks. Color code: yellow, Au; dark blue, Ir; light blue, Pd; orange, P; gray, C.

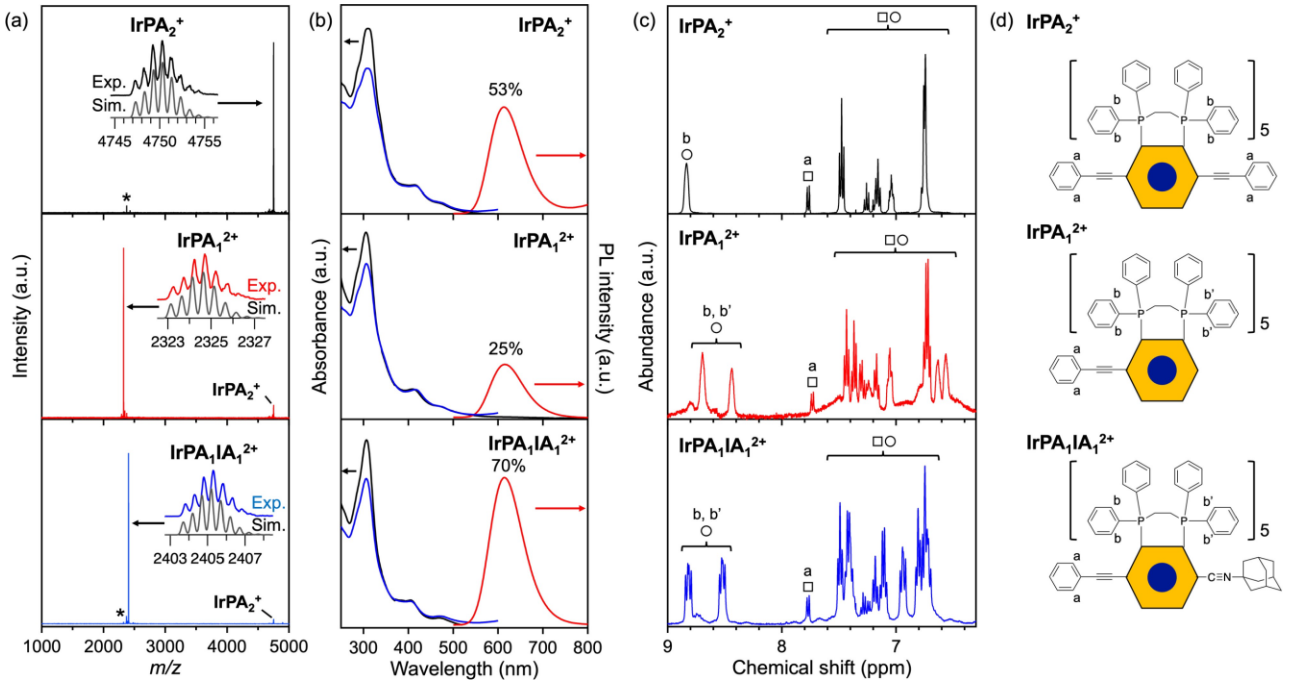

Figure 2. (a) ESI mass spectra of the acetonitrile solutions of $\mathbf{IrPA_2}^{+}$ (black), a mixture of $\mathbf{IrPA_2}^{+}$ and one eq. of HBF_4 (red), a mixture of $\mathbf{IrPA_1}^{2+}$ and one eq. of **IA** (blue). The insets compare the experimental and simulated isotope patterns. The small peak marked with an asterisk (*) was assigned to $[IrAu_{12}(dppe)_5(PA)_2]^{2+}$ (oxidized species of $\mathbf{IrPA_2}^{+}$). (b) Absorption (black), photoluminescence (red; λ_{ex} = 415 nm), and excitation (blue; λ_{em} = 615 nm) spectra of $\mathbf{IrPA_2}^{+}$, $\mathbf{IrPA_1}^{2+}$, and $\mathbf{IrPA_1IA_1}^{2+}$. (c) ^1H NMR (400 MHz) charts of $\mathbf{IrPA_2}^{+}$ (black), $\mathbf{IrPA_1}^{2+}$ (red), and $\mathbf{IrPA_1IA_1}^{2+}$ (blue). The charts of $\mathbf{IrPA_2}^{+}$ and $\mathbf{IrPA_1IA_1}^{2+}$ were measured in acetone-*d*6, while that of $\mathbf{IrPA_1}^{2+}$ was measured in acetonitrile-*d*3. The circles and squares indicate the signals from dppe and PA ligands, respectively. (d) Assignment of protons in $\mathbf{IrPA_2}^{+}$, $\mathbf{IrPA_1}^{2+}$, and $\mathbf{IrPA_1IA_1}^{2+}$. The yellow hexagon with a blue circle at the center represents the $IrAu_{12}$ core.

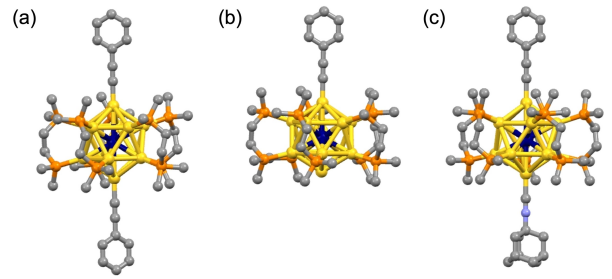

Figure 3. DFT-optimized structures of (a) **IrPA$_2$-m^{+}**, (b) **IrPA$_1$-m^{2+}**, and (c) **IrPA$_1$IA$_1$-m^{2+}**. Hydrogens are omitted for clarity. The color code is the same as in Figure 1 except blue for N.

ure S4a), the highest occupied molecular orbital (HOMO) consisted of the combination of the 1P superatomic orbital of the Ir@Au$_{12}$ core and the π orbital of the PA ligands, while the lowest unoccupied molecular orbital (LUMO) mainly consisted of the 1D superatomic orbital. Thus, **IrPA$_2^{+}$** can be viewed as an Ir@Au$_{12}$(8e) superatom modified with dppe and PA ligands.

Desorption of Alkynyl Ligand by Acid

Cluster **IrPA$_2^{+}$** was chosen as an initial target expecting that the Au–C bonds would be more easily dissociated than those in **AuPA$_2^{3+}$** and **PdPA$_2^{2+}$** based on the Au–C bond length. We first studied the reaction of **IrPA$_2^{+}$** with various Brønsted acids (Table 1)[28–34] in acetonitrile (AN) using ESI-MS. **IrPA$_2^{+}$** was almost completely converted to [IrAu$_{12}$(dppe)$_5$(PA)$_1$]$^{2+}$ (**IrPA$_1^{2+}$**) by adding one equivalent of strong acids such as HBF$_4$ (Figure 2a, red), trifluoroacetic acid (TFA–H) (Figure S5a), and 10-camphorsulfonic acid (CSA–H) (Figure S5b). In contrast, **IrPA$_1^{2+}$** was not produced when weaker acids such as chloroacetic acid (CH$_2$ClCOOH) and acetic acid (CH$_3$COOH) were added (Figures S5c and S5d). These results suggest that sufficiently strong acids can remove a PA ligand from the Ir@Au$_{12}$ core of **IrPA$_2^{+}$**. Given that the p*K*a value of PA–H in water is 23.2,[35] the formation of **IrPA$_1^{2+}$** can be viewed as the release of a weak acid (PA–H) from **IrPA$_2^{+}$** by a strong acid (H^{+}X^{-}) as follows:

Table 1: Reaction products with **IrPA$_2^{+}$** and one equivalent of various acids

Acid	p*K*a in H$_2$O	p*K*a in AN	Product[a]
HBF$_4$	−4.9[b]	1.8[c]	**IrPA$_1^{2+}$**
TFA-H	0.59 or 0.32[b]	12.7[d]	**IrPA$_1^{2+}$**
CSA-H	1.2[e]	–[f]	**IrPA$_1^{2+}$**
CH$_2$ClCOOH	2.85[g]	18.8[h]	**IrPA$_2^{+}$**
CH$_3$COOH	4.76[g]	22.3[i]	**IrPA$_2^{+}$**

[a]The main product observed in the ESI mass spectrum. [b]Ref. [28]. [c]Ref. [29]. [d]Ref. [30]. [e]Ref. [31]. [f]Not available. [g]Ref. [32]. [h]Ref. [33]. [i]Ref. [34].

$$\mathbf{IrPA_2}^{+} + \mathrm{H^+X^-} \rightarrow \mathbf{IrPA_1}^{2+} + \mathrm{PA{-}H} + \mathrm{X^-} \quad (1)$$

The key step of eq. (1) may be weakening of the Au–C bond via protonation of the C≡C bond of the PA ligand, but further work is needed to elucidate the detailed mechanism. When one equivalent of HCl was mixed with **IrPA$_2^{+}$**, [IrAu$_{12}$(dppe)$_5$(PA)$_1$Cl$_1$]$^{+}$ (**IrPA$_1$Cl$_1^{+}$**) was generated (Figure S6), indicating that low coordination ability of the conjugate base X^{-} to gold is also necessary to leave the site open.

The new product, **IrPA$_1^{2+}$**, was characterized in more detail. The UV/Vis absorption and PL spectra of **IrPA$_1^{2+}$** are similar to those of **IrPA$_2^{+}$** (Figure 2b), indicating that the removal of PA from **IrPA$_2^{+}$** does not appreciably change its geometric structure. This conclusion was further supported by the similarity of the DFT-optimized structures of **IrPA$_2$-m^{+}** (Figure 3a) and [IrAu$_{12}$(dmpe)$_5$(PA)$_1$]$^{2+}$ (**IrPA$_1$-m^{2+}**) (Figure 3b). The exposure of a single Au atom on the Ir@Au$_{12}$ surface is illustrated by a space-filling representation of **IrPA$_1$-m^{2+}** (Figure S7a). A superatom-like electronic structure was retained in **IrPA$_1$-m^{2+}** although the energy levels and shapes of the KS orbitals were slightly different from those of **IrPA$_2$-m^{+}** (Figure S4b). In contrast, the PL QY was significantly reduced from 53 % to 25 % upon the removal of one PA (Figure 2b, red). This PL quenching is ascribed to the acceleration of the nonradiative relaxation of the photoexcited states of **IrPA$_1^{2+}$** due to poor ligand packing around the Ir@Au$_{12}$ core. ^{1}H NMR spectroscopy (red trace in Figure 2c, Figure S8) revealed that the single peak at ~8.8 ppm (peak b) for **IrPA$_2^{+}$** was split into two (peaks b and b') in **IrPA$_1^{2+}$** (~8.4 and ~8.7 ppm), reflecting the inequivalent environment of the phenyl groups of dppe upon removal of one PA (b and b' in Figure 2d). The stability of **IrPA$_1^{2+}$** in AN solution was confirmed by UV/Vis spectroscopy and ESI-MS as a function of storage time (Figure S9). Both measurements suggested that **IrPA$_1^{2+}$** did not decompose after storage for at least 1 week at room temperature in the dark.

The remaining PA of **IrPA$_1^{2+}$** could be removed by adding four equivalents of HBF$_4$ to the AN solution of **IrPA$_2^{+}$**. ESI-MS detected [IrAu$_{12}$(dppe)$_5$]$^{3+}$ (**Ir^{3+}**) without PA ligands along with the adducts with AN solvent and BF$_4^{-}$ anion (Figure S10). The DFT-optimized structure of [IrAu$_{12}$(dmpe)$_5$]$^{2+}$ (**Ir-m^{3+}**) (Figure S7b) predicts that **Ir^{3+}** has two open sites at opposite positions of the Ir@Au$_{12}$ core. The KS orbitals of **Ir-m^{3+}** (Figure S4c) show that HOMO and HOMO-1 correspond to 1P superatomic orbitals. These results demonstrate that open sites can be created in a controlled manner on the IrAu$_{12}$ superatomic core by acid-induced PA release.

Then, the scope of the acid-induced PA removal was examined for the other clusters **PdPA$_2^{2+}$** and **AuPA$_2^{3+}$** by using the strongest acid HBF$_4$. The PA removal proceeded partly from **PdPA$_2^{2+}$**, but not from **AuPA$_2^{3+}$** (Figure S11). Thus, the reactivity of **MPA$_2$** with acid is reduced in the order of **IrPA$_2^{+}$**, **PdPA$_2^{2+}$**, and **AuPA$_2^{3+}$**, which is parallel to the order of Au–C bond length. The selective removal of PA from **IrPA$_2^{+}$** is probably associated with the weaker

Au–C bond and smaller electrostatic repulsion between the monocationic $\mathbf{IrPA_2}^{+}$ and H^+ compared to that between the doubly and triply charged $\mathbf{PdPA_2}^{2+}$ and $\mathbf{AuPA_2}^{3+}$, respectively.

Reactivity of the Open Site

DFT calculations predicted that the LUMO of $\mathbf{IrPA_1\text{-}m}^{2+}$ has a large lobe on the exposed site of the core (Figure S4b), implying that the open site of $\mathbf{IrPA_1}^{2+}$ can accommodate nucleophiles. This hypothesis was tested by a trapping experiment. $\mathbf{IrPA_1}^{2+}$ was completely converted to $[IrAu_{12}(dppe)_5(PA)_1(IA)_1]^{2+}$ ($\mathbf{IrPA_1IA_1}^{2+}$) upon the addition of one equivalent of 1-isocyanoadamantane (IA) (Figure 2a, blue):

$$\mathbf{IrPA_1}^{2+} + \text{CN-(adamantyl)} \ (\text{IA}) \rightarrow \mathbf{IrPA_1IA_1}^{2+} \qquad (2)$$

Further addition of IA did not proceed smoothly even when two equivalents of IA were added (Figure S12). As a control, direct mixing of $\mathbf{IrPA_2}^{+}$ with one or two equivalents of IA was conducted. Small amounts of $\mathbf{IrPA_1IA_1}^{2+}$ and $[Au(dppe)_2]^+$ were detected, while the majority of $\mathbf{IrPA_2}^{+}$ remained unreacted (Figure S13). These results indicate that the open site of $\mathbf{IrPA_1}^{2+}$ can be efficiently and selectively occupied by a single IA molecule. The absorption and PL spectra of $\mathbf{IrPA_1IA_1}^{2+}$ remained similar to those of $\mathbf{IrPA_1}^{2+}$, respectively (Figure 2b), indicating that the superatomic nature was retained during the coordination of IA. However, the PL QY was significantly enhanced from 25 % to 70 % by the incorporation of IA to $\mathbf{IrPA_1}^{2+}$, probably due to the rigidification of the $IrAu_{12}$ core by the completion of the densely packed ligand layer in $\mathbf{IrPA_1IA_1}^{2+}$. The ^{1}H NMR chart of $\mathbf{IrPA_1IA_1}^{2+}$ (Figure 2c, blue) exhibited similar patterns to those of $\mathbf{IrPA_1}^{2+}$, indicating that the geometric structure of the dppe ligand layer was hardly changed by the IA ligation. The DFT optimized structure of $[IrAu_{12}(dmpe)_5(PA)_1(IA)_1]^{2+}$ ($\mathbf{IrPA_1IA_1\text{-}m}^{2+}$) in Figure 3c and S7c illustrates that IA is coordinated to the open site of $\mathbf{IrPA_1\text{-}m}^{2+}$ while retaining the core structure. The superatomic electronic structure of $\mathbf{IrPA_1IA_1}^{2+}$ was supported by KS orbitals of $\mathbf{IrPA_1IA_1\text{-}m}^{2+}$ (Figure S4d). Gibbs free energies calculated for $\mathbf{IrPA_1\text{-}m}^{2+} + IA \rightarrow \mathbf{IrPA_1IA_1\text{-}m}^{2+}$ and $\mathbf{IrPA_2\text{-}m}^{+} + IA \rightarrow \mathbf{IrPA_1IA_1\text{-}m}^{2+} + PA^-$ were -0.5 and $+5.6$ eV, respectively, at $T = 298$ K. This estimation explains why the IA could not be introduced by the ligand exchange, but by the coordination to the open site of $\mathbf{IrPA_1}^{2+}$.

Controlled Linkage of the $IrAu_{12}$ Superatoms

Efficient coordination of isocyanide (IA) to the open site of $\mathbf{IrPA_1}^{2+}$ suggests that multiple $\mathbf{Ir}^{3+}$ can be connected using diisocyanide, such as 4″-*p*-terphenyldiisocyanide (L), as a linker. The resulting oligomers are expected to have a linear configuration because the open sites of $\mathbf{Ir}^{3+}$ are located at the coaxial position of the icosahedral $IrAu_{12}$ core. Furthermore, the number of $IrAu_{12}$ superatoms linked can be controlled using L, $\mathbf{Ir}^{3+}$ and $\mathbf{IrPA_1}^{2+}$ as building units according to a strategy shown in Scheme 1. The first step is the synthesis of the dimer and trimer of the $IrAu_{12}$ superatoms as shown in Scheme 1a and 1b, respectively. The dimer is formed by addition of 0.5 eq. of L to $\mathbf{IrPA_1}^{2+}$ (step i), while the trimer is formed by sequential addition of two equivalents of L (step i) and two equivalents of $\mathbf{IrPA_1}^{2+}$ (step ii) to $\mathbf{Ir}^{3+}$. Two $IrAu_{12}$ superatoms can be added to both ends of the dimers or trimers by acid-induced removal of two PA ligands from both sides (step iii), followed by steps i and ii. By repeating these three steps, targeted synthesis of multimers with any number of constituents is possible in principle.

To demonstrate the applicability of this strategy, we herein show the synthetic results of the dimer and trimer of $IrAu_{12}$ superatoms. According to Scheme 1a, 0.5 equivalent of L was added to the solution of $\mathbf{IrPA_1}^{2+}$. The ESI mass spectrum of the purified products (Figure 4a, red) was dominated by the peak of the target dimer $\mathbf{(IrPA_1}^{2+}\mathbf{)_2L_1}$. In the ^{1}H NMR chart (Figure 4c, red), new signals composed of one singlet and two doublet peaks (peaks c–e) appeared in the range of 7.95–8.10 ppm, in addition to those from dppe (peaks b and b') and PA (peak a) of the $\mathbf{IrPA_1}$ moieties. These new peaks are assigned to L in $\mathbf{(IrPA_1}^{2+}\mathbf{)_2L_1}$ due to the similarity with the ^{1}H NMR chart of free L (Figure S14). This assignment was further supported by the agreement between the ratio of integral areas for peaks a: b + b': c–e (1.0: 11.6: 2.8) and the number of the corresponding protons of the model structure for $\mathbf{(IrPA_1}^{2+}\mathbf{)_2L_1}$ (4H, 40H, 12H, respectively: Figure 4d). The splitting pattern of peaks c–e indicates that the protons of L in $\mathbf{(IrPA_1}^{2+}\mathbf{)_2L_1}$ were in three different environments, which is explained by the model structure shown in Figure 4d.

Transmission electron microscopy (TEM) measurement was conducted to visualize the linked structure of $\mathbf{(IrPA_1}^{2+}\mathbf{)_2L_1}$. We attempted to align $\mathbf{(IrPA_1}^{2+}\mathbf{)_2L_1}$ along the boron nitride nanotubes (BNNTs) in the hope of observing

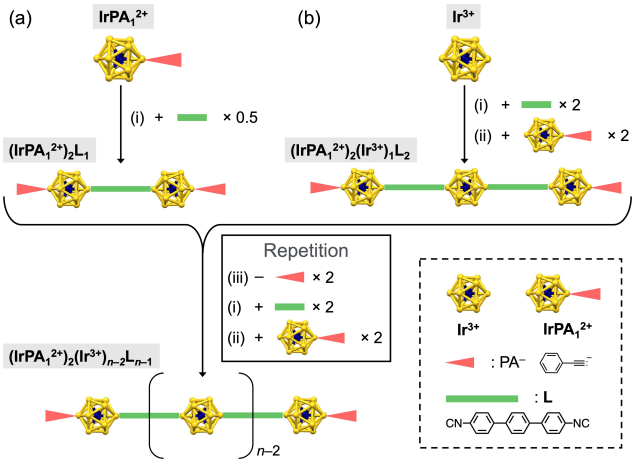

Scheme 1. Synthetic scheme of (a) even- and (b) odd-numbered oligomers of $Ir@Au_{12}$ superatoms. The building blocks are shown in the legend.

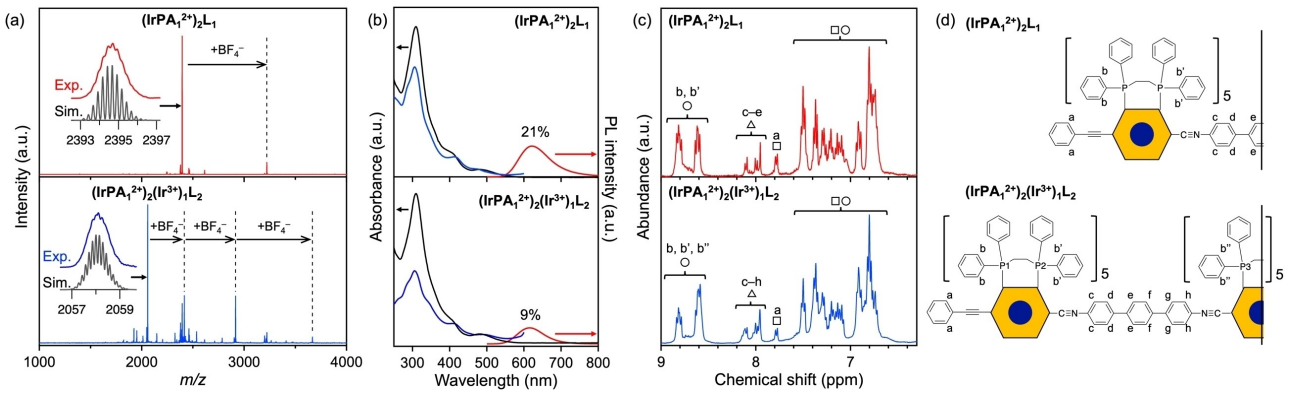

Figure 4. (a) ESI mass spectra of the acetonitrile solutions of **$(IrPA_1^{2+})_2L_1$** (red) and **$(IrPA_1^{2+})_2(Ir^{3+})_1L_2$** (blue). The insets compare the experimental and simulated isotope patterns. (b) Absorption (black), photoluminescence (red; $\lambda_{ex}=415$ nm), and excitation (blue; $\lambda_{em}=615$ nm) spectra of **$(IrPA_1^{2+})_2L_1$** and **$(IrPA_1^{2+})_2(Ir^{3+})_1L_2$**. (c) ^{1}H NMR (400 MHz) charts of **$(IrPA_1^{2+})_2L_1$** (red) and **$(IrPA_1^{2+})_2(Ir^{3+})_1L_2$** (blue), which were measured in acetone-*d*6. The circles, squares, and triangles indicate the signals from dppe, PA, and L ligands, respectively. (d) Schematic illustration of **$(IrPA_1^{2+})_2L_1$** and **$(IrPA_1^{2+})_2(Ir^{3+})_1L_2$**. The yellow hexagons containing a blue circle represent the $IrAu_{12}$ core.

TEM images from a direction perpendicular to the interparticle bond. Figures 5 and S15 represent TEM images of selected areas of the sample thus prepared. The blurred images of the $IrAu_{12}$ particles are due to dynamic structural change during the exposure time of the TEM imaging. The average center-to-center distance between the $IrAu_{12}$ cores was 2.7 nm, which agrees well with the sum of the diameter of **$IrPA_1^{2+}$** (0.8 nm) and the length of L (1.9 nm). These results suggest that two **$IrPA_1^{2+}$** units are successfully linked by L.

The trimer was synthesized in two steps according to Scheme 1b: mixing **Ir^{3+}** and two equivalents of L, followed by capping both ends by two equivalents of **$IrPA_1^{2+}$**. In the ESI mass spectrum (Figure 4a, blue), the target trimer **$(IrPA_1^{2+})_2(Ir^{3+})_1L_2$** and adducts of BF_4^- were observed as the main products, while a small amount of the dimers and tetramers was observed as impurities (Figure S16). In the ^{1}H NMR spectrum (Figure 4c, blue), the relative intensity of doublet peaks at 8.6 and 8.8 ppm from dppe (peaks b, b', and b") is significantly different from that of the dimer (peaks b and b' in the red trace of Figure 4c). This behavior was explained by the overlap of the doublet peaks at ~8.6 and ~8.8 ppm from dppe on the terminal $IrAu_{12}$ cores (b and b' in Figure 4d; 20H and 20H, respectively) and the singlet peak at 8.6 ppm from dppe on the central $IrAu_{12}$ core (b" in Figure 4d; 20H). The signals from L (peak c–h, 24H) and PA (peak a; 4H) in the trimer (Figure 4c, blue) were similar to those in the dimer (Figure 4c, red). The $^{31}P\{^1H\}$ NMR spectrum (Figure S17) exhibited a singlet and two doublet peaks, indicating that P atoms in the trimer are under three different environments. One singlet is assigned to the P atoms of the dppe ligand on the central $IrAu_{12}$ core (P3 in Figure 4d), and two doublets are assigned to the P atoms of the dppe ligands on the terminal $IrAu_{12}$ cores (P1 and P2 in Figure 4d). These results indicate that the linear trimer was successfully synthesized with high purity.

The absorption spectrum of **$(IrPA_1^{2+})_2(Ir^{3+})_1L_2$** (Figure 4b, black) was very similar to that of **$(IrPA_1^{2+})_2L_1$**, but their spectral onsets are redshifted as compared to that of **$IrPA_1IA_1^{2+}$** unit (Figure S18). This result indicates that the HOMO–LUMO gap of the $IrAu_{12}$ superatom is reduced by linkage. The PL QY decreased with an increase in the linkage: 70, 21, and 9 % for **$IrPA_1IA_1^{2+}$**, **$(IrPA_1^{2+})_2L_1$**, and **$(IrPA_1^{2+})_2(Ir^{3+})_1L_2$**, respectively. These results suggest that electronic states and relaxation dynamics of the $IrAu_{12}$ superatom are affected by the neighboring $IrAu_{12}$ unit(s) through linker L. The degree of perturbation might be dependent on the number and/or distance of the constituent units and the electronic nature of linking ligands, which will be a target of future study.

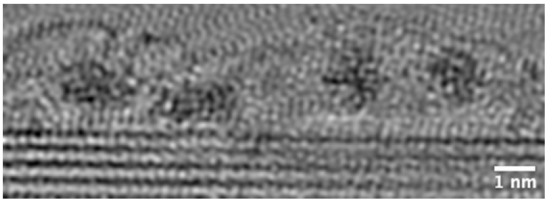

Figure 5. TEM image of **$(IrPA_1^{2+})_2L_1$** on BNNT.

Conclusion

We herein report a method for making atomically precise open sites on chemically modified gold superatoms with well-defined structures. Controlled amounts of strong Brønsted acid removed one or two PA ligands from $[IrAu_{12}(dppe)_5(PA)_2]^+$ leaving the superatomic $IrAu_{12}$ core intact. A single isocyanide was selectively coordinated to the exposed site of $[IrAu_{12}(dppe)_5(PA)_1]^{2+}$. Furthermore, the dimer and linear trimer of $IrAu_{12}$ superatoms were selectively synthesized by linking $[IrAu_{12}(dppe)_5(PA)_1]^{2+}$ and $[IrAu_{12}(dppe)_5]^{3+}$ by diisocyanide. The linkage of the superatoms with the predesigned coordination site(s) proposed here is superior to the conventional ligand-exchange approach in terms of the controllability of the length and

direction of the assembly. This study provides the basis for fabricating the exposed sites on Au CMSs for various applications, such as programable assembly and selective catalysis.

Acknowledgements

We thank Prof. Tomohiro Shiraki (Kyushu University) for providing us with purified BNNT for the TEM observation, and Dr. Koji Kimoto (NIMS) for his assistance with the 40 kV TEM observation. This research was financially supported by JST, CREST (Grant No. JPMJCR20B2) and by JSPS KAKENHI Grants (Nos. JP20H00370, JP23H00284, JP23H01917, and JP23H04874).

Conflict of Interest

The authors declare no conflict of interest.

Data Availability Statement

The data that support the findings of this study are available from the corresponding author upon reasonable request.

Keywords: ligand desorption reaction · phosphine-protected gold superatoms · programmed assembly

[1] R. Jin, C. Zeng, M. Zhou, Y. Chen, *Chem. Rev.* **2016**, *116*, 10346–10413.
[2] I. Chakraborty, T. Pradeep, *Chem. Rev.* **2017**, *117*, 8208–8271.
[3] Y. Du, H. Sheng, D. Astruc, M. Zhu, *Chem. Rev.* **2020**, *120*, 526–622.
[4] S. Takano, T. Tsukuda, *J. Am. Chem. Soc.* **2021**, *143*, 1683–1698.
[5] P. Chakraborty, A. Nag, A. Chakraborty, T. Pradeep, *Acc. Chem. Res.* **2019**, *52*, 2–11.
[6] X. Kang, M. Zhu, *Coord. Chem. Rev.* **2019**, *394*, 1–38.
[7] Z. Wu, Q. Yao, S. Zang, J. Xie, *ACS Materials Lett.* **2019**, *1*, 237–248.
[8] A. Ebina, S. Hossain, H. Horihata, S. Ozaki, S. Kato, T. Kawawaki, Y. Negishi, *Nanomaterials* **2020**, *10.* 1105.
[9] Y. Saito, C. Murata, M. Sugiuchi, Y. Shichibu, K. Konishi, *Coord. Chem. Rev.* **2022**, *470*, 214713.
[10] K. Sokolowska, E. Hulkko, L. Lehtovaara, T. Lahtinen, *J. Phys. Chem. C* **2018**, *122*, 12524–12533.
[11] A. Sels, G. Salassa, F. Cousin, L.-T. Lee, T. Bürgi, *Nanoscale* **2018**, *10*, 12754–12762.
[12] Y. Saito, Y. Shichibu, K. Konishi, *Nanoscale* **2021**, *13*, 9971–9977.
[13] M. Swierczewski, F. Cousin, E. Banach, A. Rosspeintner, L. M. Lawson Daku, A. Ziarati, R. Kazan, G. Jeschke, R. Azoulay, L.-T. Lee, T. Bürgi, *Angew. Chem. Int. Ed.* **2023**, *62*, e202215746.
[14] V. Sudheeshkumar, K. O. Sulaiman, R. W. J. Scott, *Nanoscale Adv.* **2020**, *2*, 55–69.
[15] T. Kawawaki, Y. Kataoka, M. Hirata, Y. Iwamatsu, S. Hossain, Y. Negishi, *Nanoscale Horiz.* **2021**, *6*, 409–448.
[16] Z.-J. Guan, J.-J. Li, F. Hu, Q.-M. Wang, *Angew. Chem. Int. Ed.* **2022**, *61*, e202209725.
[17] N. de Silva, J.-M. Ha, A. Solovyov, M. M. Nigra, I. Ogino, S. W. Yeh, K. A. Durkin, A. Katz, *Nat. Chem.* **2010**, *2*, 1062–1068.
[18] J. Chen, Q.-F. Zhang, T. A. Bonaccorso, P. G. Williard, L.-S. Wang, *J. Am. Chem. Soc.* **2014**, *136*, 92–95.
[19] S.-F. Yuan, Z. Lei, Z.-J. Guan, Q.-M. Wang, *Angew. Chem. Int. Ed.* **2021**, *60*, 5225–5229.
[20] Y. Li, H. K. Kim, R. D. McGillicuddy, S.-L. Zheng, K. J. Anderton, G. J. Stec, J. Lee, D. Cui, J. A. Mason, *J. Am. Chem. Soc.* **2023**, *145*, 9304–9312.
[21] M. Sugiuchi, Y. Shichibu, T. Nakanishi, Y. Hasegawa, K. Konishi, *Chem. Commun.* **2015**, *51*, 13519–13522.
[22] Y. Shichibu, K. Konishi, *Small* **2010**, *6*, 1216–1220.
[23] H. Hirai, S. Takano, T. Nakamura, T. Tsukuda, *Inorg. Chem.* **2020**, *59*, 17889–17895.
[24] H. Hirai, S. Takano, T. Nakashima, T. Iwasa, T. Taketsugu, T. Tsukuda, *Angew. Chem. Int. Ed.* **2022**, *61*, e202207290.
[25] See Supporting Informtaion for details.
[26] Deposition Number 2325124 contains the supplementary crystallographic data for this paper. These data are provided free of charge by the joint Cambridge Crystallographic Data Centre and Fachinformationszentrum Karlsruhe Access Structures service www.ccdc.cam.ac.uk/structures.
[27] Deposition Number 2278390 contains the supplementary crystallographic data for this paper. These data are provided free of charge by the joint Cambridge Crystallographic Data Centre and Fachinformationszentrum Karlsruhe Access Structures service www.ccdc.cam.ac.uk/structures.
[28] Fluorine Compounds. In *Kirk-Othmer Encyclopedia of Chemical Technology*, 4th ed.; Wiley, 1994; Vol. 11, pp 309 and 547.
[29] A. Kütt, T. Rodima, J. Saame, E. Raamat, V. Mäemets, I. Kaljurand, I. A. Koppel, R. Y. Garlyauskayte, Y. L. Yagupolskii, L. M. Yagupolskii, E. Bernhardt, H. Willner, I. Leito, *J. Org. Chem.* **2011**, *76*, 391–395.
[30] Y. Hayakawa, T. Iwase, E. J. Nurminen, M. Tsukamoto, M. Kataoka, *Tetrahedron* **2005**, *61*, 2203–2209.
[31] F. F. F. Garrudo, R. N. Udangawa, P. R. Hoffman, L. Sordini, C. A. Chapman, P. E. Mikael, F. A. Ferreira, J. C. Silva, C. A. V. Rodrigues, J. M. S. Cabral, J. M. F. Morgado, F. C. Ferreira, R. J. Linhardt, *Mater. Today Chem.* **2019**, *14.* 100185.
[32] Acetic Acid and Derivatives. In *Kirk-Othmer Encyclopedia of Chemical Technology*, 4th ed.; Wiley, **1991**; Vol. 11, pp 125 and 165.
[33] M. K. Chantooni Jr, I. M. Kolthoff, *J. Phys. Chem.* **1975**, *79*, 1176–1182.
[34] I. M. Kolthoff, M. K. Chantooni Jr, *J. Am. Chem. Soc.* **1975**, *97*, 1376–1381.
[35] A. Streitwieser Jr, D. M. E. Ruben, *J. Am. Chem. Soc.* **1971**, *93*, 1794–1795.

Manuscript received: January 29, 2024
Accepted manuscript online: February 9, 2024
Version of record online: February 28, 2024